Author's Copy: J.B. Bancroft, A. Morrison, G. Lachapelle, Validation of GNSS under 500,000 V Direct Current (DC) transmission lines, Computers and Electronics in Agriculture, Volume 83, April 2012, Pages 58-67, ISSN 0168-1699, 10.1016/j.compag.2012.01.013. See http://dx.doi.org/10.1016/j.compag.2012.01.013

Validation of GNSS under 500,000 Volt Direct Current (DC) Transmission Lines

J.B. Bancroft*, A. Morrison and G. Lachapelle

j.bancroft@ucalgary.ca, ajmorris@ucalgary.ca, gerard.lachapelle@ucalgary.ca

Position, Location and Navigation Group, Schulich School of Engineering, University of Calgary

2500 University Drive, NW, Calgary, Alberta T2N 1N4, Canada

Phone Number: 001 403 210 9802

*Corresponding Author

Abstract

The use of Global Navigation Satellite Systems (GNSS) is common amongst agricultural users and enables the producer to optimize crop production within soil variant fields to provide better farming practices. Many agricultural navigation systems are dependent on real time GNSS navigation solutions to aid and control farm machinery. Direct current (DC) and Alternating Current (AC) transmission lines overhead are often suspected to create interference with GNSS equipment preventing farmers from utilizing their GNSS supported equipment. This paper provides evidence that only non-impeding effects on the receiver or incoming signals, in the form of cycle slips, were measured or detected from either the overhead lines and/or their corresponding support towers. No effect on code measurements was detected. The latter effect is due to reflection or brief masking by the towers. Tests were conducted under a set of three transmission lines, two 500 kV DC lines and one 230 kV AC line. Several GNSS receivers and processing methods, including real time and post-processed data, are used to measure and process data to study the position accuracy, dilution of precision, number of satellites tracked, code and phase errors, location and number of carrier phase cycle slips, carrier-to-noise density and L1-L2 carrier divergence. One commercial Real Time Kinematic (RTK) survey system was also used to verify the 450 MHz data link was operational.

Keywords: GNSS, High Voltage Transmission Lines, Interference, Precision Agriculture, Direct Current

1. Introduction and Background

Agricultural and survey grade GNSS receivers within farming equipment are often used for automated steering, custom geographic seeding and fertilizing and harvest yield mapping. These systems are often dependent on real time GNSS receivers operating with centimetre accuracy. Code and carrier phase measurements made by the receivers are used to obtain such a high accuracy level. These systems often utilize real time corrections from an additional static receiver or from other satellite or terrestrial based systems (e.g. Omnistar or the United States Coast Guard (USCG) Differential GPS Network). Thus, the issue of operating agricultural and survey grade GNSS equipment has three potential failures: the GNSS satellite network, the receiver itself or the additional communication system providing real time corrections (or data) to the moving receiver. This paper provides an in depth analysis of GNSS receivers tracking and navigation performance beneath 500 kV DC lines and confirming the correct operation of a single commercially available 450 MHz data link.

Regarding the issue of GNSS interference from overhead high voltage transmission lines, Silva & Olsen (2002) presented some results for 120 and 345 kV AC lines. Using a single Trimble GPS receiver of that period, they observed no adverse effects on the carrier to noise density of the incoming signal. Since signal strength alone cannot determine the full impact of multipath signals r the lines and their corresponding towers more analysis in the observation and position

domains is required. Silva (2002) discussed the effect of interference on the communication link between 283.5 - 325 kHz, which is the band where the USCG DGPS network broadcasts corrections. Although the effects at this frequency are beyond the scope of this paper, the author concludes that there is minimal impact on the data link resulting from high voltage transmission lines in the 283.5 - 325 kHz band. Phaiboon et al (2000) provides a novel survey of interference from 500 kV transmission lines. The paper addresses interference with the 0.5 - 100 MHz band, but concludes that higher band frequencies (such as GPS L1 at 1575 MHz) should experience no effect.

The origins and effects of corona discharge are described by Juette (1971), Pacific Gas and Electric (2005) and Phillips (2007). While it is generally believed that transmission line noise is not typically observable above 1 MHz, Juette (1971) has shown that interference is possible even on much higher frequency signals. For this reason one must consider the possibility that interference may be observed at GNSS signal populated frequency bands.

The locally ionized atmosphere around the high voltage conductors as discussed by Pacific Gas and Electric (2005) could be superficially compared to the naturally occurring ionized atmosphere in the ionosphere, however the direct calculation of this field is extremely challenging. The mechanism by which a current of charged particles could flow between the conductors of a transmission line system must be due to one of the three possible modes of current flow. Conduction current as defined by Sadiku (2001) requires the satisfaction of Ohms law whereby the current density in the conductor $\mathbf{J}$ is equal to the product of the material conductivity σ and the applied electric field $\mathbf{E}$. Since a conductor is defined as having a σ approaching infinity, this implies an electric field within the conductor is approaching zero. Further, Gauss Law states that if the electric field intensity is zero ($\mathbf{E}=0$), the charge density within the conductor ρ_v must also be zero (Sadiku 2001, pp.165). Obviously, since air is not a conductor, the leakage current between the transmission line conductors must be explained by phenomena other than conduction.

1.1 Displacement Current

The concept of displacement current $\mathbf{J}_d$ is very important in radio frequency applications, as it is the displacement current which explains the propagation of electromagnetic waves through free space (Sadiku 2001, pp. 382). Considering the long spans of parallel transmission line cable to the plates of a capacitor, it is conceptually possible to explain the presence and flow of leakage current between the conductors as being a manifestation of the displacement current. While this would imply that the integral of the magnetic field intensity $\mathbf{H}$ with respect to the flow of current I over any closed surface $\mathbf{S}$ between the two conductors taken along a path L would be equal to the surface integral of the conduction current density $\mathbf{J}$ as shown in Equation (1), it is already known that $\mathbf{J}$ is zero for a non-conducting medium such as air.

$$\oint_L \mathbf{H}\bullet d\mathbf{l} = \int_S \mathbf{J}\bullet d\mathbf{S} = I \qquad (1)$$

However, since the conduction current $\mathbf{J}$ is known to be zero in non-conducting air, the total current density is redefined as the conduction current $\mathbf{J}$ plus the displacement current $\mathbf{J}_d$. Thus Ampere's circuit law involves the time rate of change of the electrical flux density $\mathbf{D}$ (Sadiku 2001, pp. 383) as shown below to produce the time rate of displacement of charge Q.

$$\oint_L \mathbf{H}\bullet d\mathbf{l} = \int_S \mathbf{J}_d \bullet d\mathbf{S} = \frac{d}{dt}\int_S \mathbf{D}\bullet dS = \frac{dQ}{dt} = I \,. \qquad (2)$$

The conclusion is that the displacement current cannot be responsible for the flow of charge between the High Voltage Direct Current (HVDC) lines, as the electrical flux density $\mathbf{D}$ is constant with respect to time under steady state conditions, and therefore so is the integral of it over any arbitrary surface between the conductors of an HVDC line.

1.2 Convection

A convection current is defined as a flow of current through a non-conductor medium such as a liquid or gas (Sadiku 2001, pp. 163). The mechanism of convection flow is easily understood in terms of the applied electric field intensity $\mathbf{E}$ which causes a force $\mathbf{F}$ to act on each electron in the field according to Equation (3). Any ions within the field would experience the same magnitude of force but opposite in direction

$$\mathbf{F} = -e\mathbf{E}\,. \qquad (3)$$

For each electron of mass m the average drift velocity $\mathbf{u}$ of the convection current will be related to the field intensity by Newton's law in Equation (4) (the average

change in momentum of the free electron must match the applied force (Sadiku 2001, pp.164)), where τ is the average time between collisions according to

$$\frac{m}{\tau}\mathbf{u} = -e\mathbf{E}. \quad (4)$$

Rearranging Equation (4), velocity is stated in Equation (5) as

$$\mathbf{u} = \frac{-e\tau}{m}\mathbf{E}. \quad (5)$$

If the volume charge density ρ_v is expressed per Equation (6) such that

$$\rho_v = -ne. \quad (6)$$

then the convection current density $\mathbf{J}_{con}$ is given in terms of the collision time and charged particle mass (as conductivity σ) by (Sadiku 2001, pp. 164) in Equation (7) where

$$\mathbf{J}_{con} = \rho_v\mathbf{u} = \frac{ne^2\tau}{m}\mathbf{E} = \sigma\mathbf{E}. \quad (7)$$

The conductivity of air is given by Pawar (2009) to be as low as 0.295×10^{-14} Siemens per metre, though this figure is recognized to vary with altitude, humidity, and temperature.

While the stated equations are easily applicable to theoretical problems involving infinite plane conductors at infinite distance from any other surfaces, and in the absence of moving air (wind), they quickly become intractable for the real life problem of braided transmission lines near the surface of the earth, exposed to wind. For this reason advanced computer simulation involving finite element analysis via specialized software is required to approximate the convection current, and therefore the term of interest, the charge density between such conductors. For this reason, the values published by Lundkvist et al (2009) for similar 500kV DC bipole transmission lines are accepted as a reference level for current flow rate and spatial charge density between the conductors.

The effect of the ionosphere on the propagation of navigation satellite signals is directly observable when using multiple signals at different frequencies originating from the same satellite such as the L1 and L2 civil signals from GPS and GLONASS. This is due to the charged atmospheric layers being dispersive at L-Band frequencies, thereby imparting a varying signal delay effect inversely proportional to the square of the carrier frequency as discussed in Morrison (2010):

$$\Delta S_{iono,g} = \frac{40.3 \bullet TEC}{f^2}. \quad (8)$$

In Equation (8) ΔS is the change in unit of length (metres) of the apparent signal path length, TEC (Total Electron Content) is the amount of charge encountered within a 1 m^2 column around the ray path of the signal where 10^{16} ions is one unit of TEC, and f is the carrier frequency of the signal. Since the GPS L1 carrier is located at 1575.42 MHz while the L2 carrier is located at 1227.6 MHz, this has the consequence of introducing a 16.2 cm per unit of TEC bias in the L1 range measurement and a 26.7 cm per unit of TEC (TECU) bias in the L2 range measurement. The magnitude of the effect on the carrier phase is equal, but the sign is reversed such that increasing levels of TEC appear to cause a decreasing range between the satellite and the user. By measuring the time series of the difference between the L1 and L2 carrier phase observations it is possible to measure the changes in encountered charge with a high level of certainty. This is since each TECU of charge by which the encountered charge quantity increases or decreases will cause a phase difference magnitude change of 10.5 cm between the two carriers.

Conceptually, the local ionization of the atmosphere adjacent to the high voltage conductors could cause a similar effect, however the expected ion current density of 60 nA/m^2 as discussed in Lundkvist et aL (2009), caused by a 500 kV DC line would be expected to produce a completely negligible effect on the order of microns. If one assumes that the peak referenced current density is uniform over a 1 metre vertical cross section between the bipole conductors, this would cause a GNSS signal passing through this region from directly above to encounter a charge of 60 nano Coulombs. Since one Coulomb is equivalent to 6.24×10^{18} elementary charges, the total encountered charge would be equivalent to 3.74×10^{11} elementary charges. In terms of the previously discussed units of TEC, this total encountered charge could be stated as 3.74×10^{-5} TECU. Since one TECU of encountered charge increase or decrease causes a 10.5 cm divergence between the L1 and L2 carrier measurements, the total encountered charge of 3.74×10^{-5} TECU would produce an expected carrier phase difference change of only 0.004 mm, while the absolute range error would be 0.006 mm on L1 and 0.010 mm on

L2. Since the L5 signal (1176.45 MHz) is in the same band, the effects would presumably be similar to those of L2, both in theory and in the measurement domain.

Thus, the purpose of this paper is to confirm the negligible effect of the corona effect and other potential interference and confirm that GNSS receivers can still operate correctly beneath and adjacent to 500 kV DC transmission lines. Data was collected under the lines in order to prove this hypothesis.

2. Data Collection

Figure 1 shows a picture of the test site located on the Nelson River Bipole system, operated by Manitoba Hydro in Winnipeg, Manitoba, Canada. Two visually identical 500 kV DC bipoles are located on the right side, with one parallel AC line at the left. Lines were located approximately 5 m above the ground. Data was collected over two days. During the first day of data collection the HVDC lines had a 537 MW and 531 MW load. During the second day of the data collection, the HVDC lines had 1124 MW and 1218 MW loading. Despite the loading difference, results were consistent on both days.

Figure 1 - Test Site

The GNSS receivers chosen were able to collect data from the Global Positioning System and the Russian GLONASS (Global Navigation Satellite System). Two receiver configurations were used to collect data, namely (i) commercially available GNSS receivers and (ii) a front-end to collect GNSS baseband data.

Two GNSS base stations, one utilizing a NovAtel DL-V3 receiver (FW 3.500), the other utilizing a Trimble R8 (FW 4.19) survey receiver were placed approximately 500 m (350 m on the 2nd day) from the DC bipoles, where they logged data continuously. The base stations served as reference stations for processing the data in differential mode, a mode commonly used for precise positioning applications such as those encountered in farming and construction.

The mobile equipment was installed in a vehicle and included four GNSS receiver systems, including a second NovAtel V3 (FW 3.620), a Trimble R8 (FW 4.19) rover, a high sensitivity u-blox receiver (u-blox Antaris 4, FW 5.0), and a NovAtel SPAN Inertial Navigation System (INS) system, which consisted of an LCI Inertial Measurement Unit (IMU) and a NovAtel SPAN SE GNSS receiver. Since INS's are self-contained and are not affected by external signals, they are used to further verify the accuracy and integrity of the GNSS-derived solutions.

To provide an extra dimension of certainty in the analysis of potential interference, the PLAN group's Leapfrog-II L-band RF front-end was used to collect direct observations of the GNSS signals from both GPS and GLONASS satellites in the L1 and L2 navigation bands. By collecting and digitizing the microwave frequencies it was possible to post-process the data using the PLAN group's GSNRx™ software receiver (Petovello et al 2009) and provide extensive signal analysis capabilities not output by commercial hardware based receivers. By using observations from high elevation angle satellites whose ray path intersect the transmission lines and the charged air between them during a perpendicular crossing run of the lines, direct measurement of the effect of air ionization was made possible via the aforementioned differential L1 and L2 carrier propagation rates in charged atmosphere.

The Trimble R8 receiver includes a 450 MHz data link that received corrections from the R8 base station, as long as the test vehicle remained within approximately 1 km of the base station. Since this data link operates on a frequency separate from the GNSS carrier frequencies, it was tested to ensure continuous operation during a subset of the test runs.

Data collected by the base stations included GPS and GLONASS pseudorange, carrier-phase, ephemeris and clock measurements. The Trimble R8 base station collected raw GNSS data and broadcasted corrections based on internal measurements and a temporary virtual point (the correct coordinates were determined after the data collection). The NovAtel V3 recorded all

information to an internal memory card for later post-processing use.

Data was collected in two kinematic modes where the vehicle moved at low speeds to simulate that of typical agricultural machinery, namely 10 - 20 km/h. First, a first trajectory approximately perpendicular to the transmission lines was traversed to a point approximately 500 m each side of the first HVDC bipole and second a trajectory running along the right of way, under and approximately parallel to the transmission lines was taken spanning the distance between three supporting towers. These trajectories were selected to assess any effects as a function of distance from the line.

In order to comply with the rated radio link limitation of 1 km while still allowing traversal testing under both HVDC bipoles as well as data collection parallel to and beneath multiple tower spans of the HVDC lines, the base stations were deployed at the position indicated in Figure 2.

Figure 2 - Map of test location showing location of the NovAtel V3 base stations for each day (green triangles), range of Trimble R8 450 MHz data link (blue circle), and position of HVDC bipoles 1 and 2 (black lines), position of AC Line (green lines) and trajectory throughout the day of the test vehicle (red). Base map from Google (2011).

Equipment supporting the mobile portion of the collection effort was divided between the roof of the test vehicle, depicted in Figure 3, and the cab of the truck where the operation of the navigation systems were monitored and managed.

Specific components of the test equipment installed on the vehicle roof were the Trimble R8 rover unit, the antenna for the high sensitivity GPS receiver, the NovAtel 702 GG pinwheel antenna used by the V3 mobile unit, the NovAtel SPAN INS, and the PLAN group Leapfrog-II L-Band Front-End module. The IMU component of the NovAtel SPAN SE system was deployed on the roof of the vehicle to provide a rigid and stable mounting point via four magnets.

Figure 3 - Mobile GNSS, inertial, and RF equipment elements mounted on roof of test vehicle. Trimble R8 rover unit at bottom right, high sensitivity GPS antennas on roof at right, NovAtel 702 GG dome antenna center left directly adjacent to LCI IMU (gray box) at center left.

The block diagram of the complete navigation test system suite is shown in Figure 4.

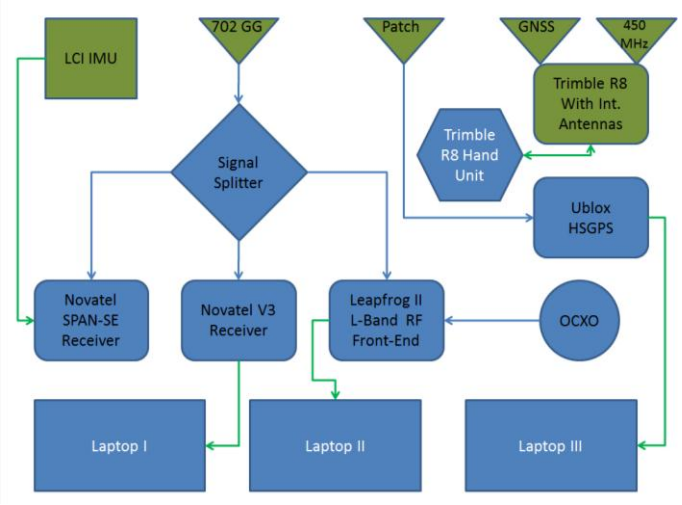

Figure 4 - Deployed equipment functional diagram. Equipment external to vehicle shown as green elements (antennas, IMU, Trimble R8), equipment

installed inside vehicle shown in blue. Cabled RF links shown with blue arrows, digital data links shown with green arrows. (For interpretation of the references to color in this figure legend, the reader is referred to the web version of this article.)

3. Data Evaluation

Nineteen segments of data were selected from the two day collection period to show key indicators of GNSS quality in real time differential and single point positioning modes. Each segment was analyzed independently and results as presented were consistent with each data segment. The exact trajectory can be seen in Figure 2, where the east/west trajectory is marked in red along Highway 321. The data and figures shown herein all refer to segment 14, a traverse perpendicular to the lines on the second day. Static data and data from the north/south trajectory were included in the other segments.

Data was processed with six different software packages. The Trimble R8 receiver combination operating in real time, in double difference ambiguity fix mode via the internal 450 MHz data link. Table 1 provides the details of each processing software package.

The reference solution was determined using a NovAtel INS. Since the INS derives its relative position from internal sensors not sensitive to electromagnetic interference of the overhead lines, this system provides an independent verification of the truth solution used.

Table 1 - Software processing strategies.

The system operated using GNSS observations to provide an absolute position. NovAtel's Inertial Explorer was used to process the data. Data was processed in the forward and reverse directions, smoothed using an RTS smoother (Gelb 1974) and finally combined to form a final navigation solution. The reference solution provided an estimated standard deviation of better than 1.7 cm (1σ).

3.1 Trimble RTK Analysis

The position differences between the Trimble Real Time Kinematic (RTK) system and the reference trajectory are shown in Figure 5. Position differences of several centimetres are common amongst receiver manufacturers and processing software, thus the differences shown on the top of Figure 5 are completely normal. The differences are due to antenna phase center variation, projection of the reference solution to the Trimble R8 antenna phase center, carrier phase noise and multipath and differences in filtering and estimation techniques used.

The horizontal dilution of precision (HDOP) and number of satellites presented in the bottom half of Figure 5 is consistent with open sky conditions. The solution of the RTK system may, for example, reject a satellite without a fixed ambiguity, occlude some satellites near the horizon or have difficulty maintaining signal lock for a

Software	GNSS Data*	Processing Methods	Purpose
NovAtel's Inertial Explorer	IMU + L1L2 GG	Post Mission Differential, Forward/Reverse processing and RTS Smoothing	Provided reference solution
University of Calgary's PLANSoft™	L1 GG	Post Mission Differential	Provide similar processing to that of precision farming navigation equipment
University of Calgary's GSNRx™	L1L2 GG	Post Mission Single Point	Provide a clear indication of tracking capabilities and carrier anomalies if present
NovAtel`s GrafNav	L1L2 G	Post Mission Differential	Second commercial software package to confirm processing techniques
Trimble's R8 Internal RTK Solution	L1L2 GG	Real Time Differential with 450 MHz radio link	RTK, similar to those of Land Surveyors
u-blox Internal Solution	L1 G	Real Time Single Point	High Sensitivity GPS receivers used in low cost mobile devices (e.g. cell phone)

low elevation satellite. The values presented in Figure 5 show ideal data, with no reason to yield navigation impediments. An HDOP of 0.6 is among the best values currently available with a GPS+GLONASS receiver at the latitude of the tests (50.1º N).

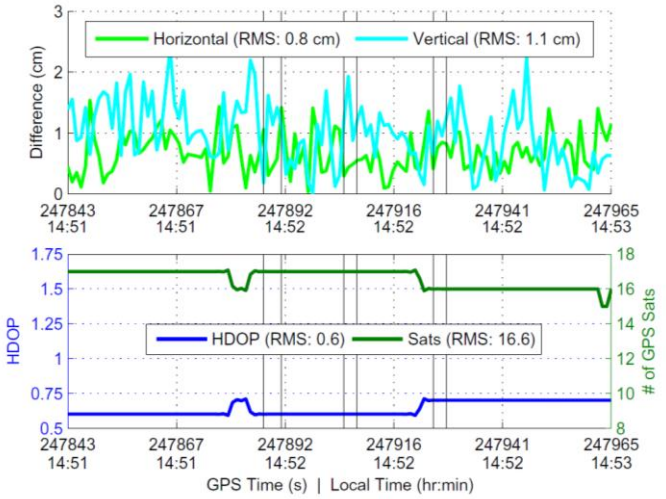

Figure 5 - Position differences and satellite geometry (vertical lines represent time directly beneath transmission lines), receiver: Trimble R8, processed by: Trimble Internal RTK Solution, data: L1 + L2 + GPS + GLONASS, test segment: 14.

Figure 6 shows the results of the data from the Trimble units, but processed with NovAtel's GrafNav software. This provides a secondary check on the data to ensure other software packages are able to fix the carrier phase ambiguities. For this test, GLONASS observations were removed to ensure that a correct GPS only solution was possible.

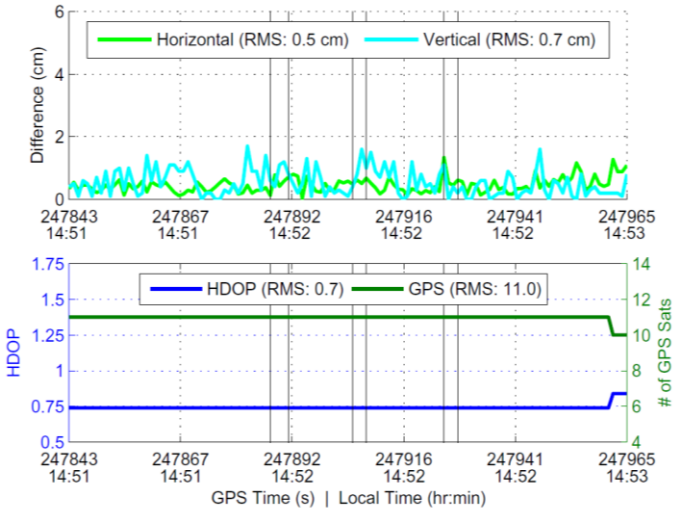

Figure 6 - Position differences and satellite geometry (vertical lines represent time directly beneath transmission lines), receiver: Trimble R8, processed by: NovAtel's GrafNav, data: L1 + L2 + GPS, test segment: 14.

3.2 NovAtel Receiver Analysis

Figure 7 shows the average carrier to noise density (C/N_0) for all satellites tracked by the NovAtel OEMV3 receiver. These results are comparable to those of open sky data and no evidence of transmission line disturbances is present. L2 signals are broadcast at 1.5 dB lower power (IS-GPS-200E 2010) than L1 and the 702GG antenna gain pattern amplifies the L2 signal 3 dB less than the L1 signal at zenith (NovAtel Inc. 2010). Further, the antenna gain pattern rolls off more rapidly on L2 than on L1, the consequence of which is the several dB lower signal level observed on L2 relative to L1. In short, a lower L2 power level is an expected effect and not a result of transmission line interference.

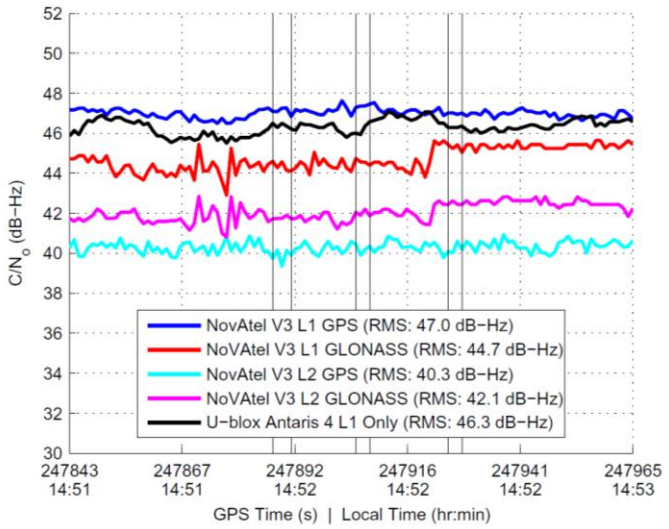

Figure 7 – GNSS signal strength (vertical lines represent time directly beneath transmission lines), receiver: NovAtel V3, data: L1 + L2 + GPS + GLONASS, test segment: 14.

Position differences as processed by PLANSoft™ are shown in Figure 8 with differences less than 1.1 cm as compared to the reference trajectory. The HDOP is exceptional throughout both segments and the number of satellites remains consistent with open sky conditions. No transmission line effect is detected as the vehicle traverses the line.

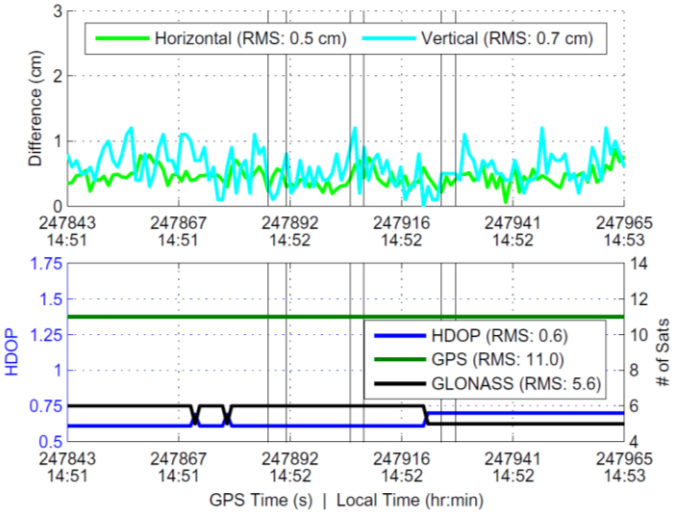

Figure 8 - Position differences and satellite geometry (vertical lines represent time directly beneath transmission lines), receiver: NovAtel V3, processed by: PLANSoft™, data: L1 + GPS + GLONASS, test segment: 14.

3.3 Residual Errors

PLANSoft™ outputs the residual error of each measurement used in the filter and residuals are often used to validate the solution. Small residuals indicate that the measurements are consistent with each other. There are additional factors that contribute to larger residuals, namely multipath and noise. Errors due to transmission line effects would result in higher residuals.

Figure 9 shows the RMS of the residuals for all measurements used within an epoch. Measurements rejected by the fault detection algorithm within the software are not used in the computation of the residual RMS. There was a minimal rejection rate (i.e. 0.067 %), a common occurrence among GNSS data gathered under open sky conditions. The rejection rate was not higher than normal due to operation under the transmission lines. Code residuals of 0.5 m and less are considered good and indicate quality observations with no hindrances. Phase residuals are also excellent at less than 1 cm. Given the number of satellites used, it is clear from this residual analysis that the receiver is functioning normally with no adverse effect from the transmission lines.

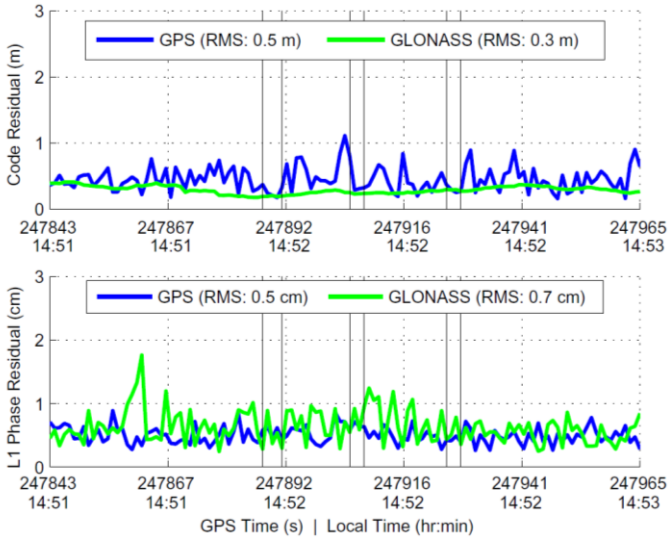

Figure 9 - RMS of residuals (vertical lines represent time directly beneath transmission lines), receiver: NovAtel V3, processed by: PLANSoft™, data: L1 + GPS + GLONASS, test segment: 14.

3.4 Carrier Phase Cycle Slip Analysis

Carrier phase cycle slips occur when the receiver loses carrier phase lock on the signals. This is commonly experienced when an obstruction blocks the direct line of sight to the signals, in which case the ambiguities affected must be re-estimated within the navigation filter. When one satellite experiences a cycle slip, the navigation filter can typically re-estimate the ambiguity within a few measurement epochs. However, if cycle slips occur on all channels simultaneously, such as when an antenna passes under an overpass, the entire ambiguity resolution process takes much longer to fix, degrading the navigation solution accuracy in the process. Thus, the number, frequency and location of cycle slips are an important metrics to analyze as they affect the navigation solution quality.

Figure 10 shows the trajectories traveled during the data collection and each cycle slip is plotted on the trajectory. Figure 10 contains all the NovAtel data collected, not just the segment analyzed (i.e. segment 14). This additional data was included to show the impact of trees on cycle slips versus the lines and towers overhead.

On the east and west ends of the data collection 362 cycle slips occurred, while only 28 cycle sips occurred beneath the transmission lines. This is due to the trees present on either side of the road, where low elevation satellites affected by these trees experience a large number of cycle slips. Some slips occur just east of the north/south trajectory where trees are present south of the road. Most importantly, although a few cycle slips occur under the lines, there is only a weak correlation between the location of the transmission line towers and the location of the cycle slips. This indicates that the transmission lines and their corresponding towers, regardless of their electric current carrying characteristics, are not causing cycle slips at a level that would impede centimetre level accuracy. Albeit cycle slips are occurring under the lines, the impact is negligible when comparing the navigation solutions to the truth solution.

It is also noteworthy that, despite a tower being located a few tens of metres from the northern most point of the data collection (where the vehicle turned to return south), no cycle slips were recorded in this area, further confirming the low effects of transmission line towers on carrier phase tracking capabilities.

Figure 10 - Geo-located cycle slips for all data collected (red: 24 January, purple: 25 January, blue tower locations).

3.5 RF Front-End Measurement Analysis

The measurements obtained from the RF front-end can be used to derive L1-L2 carrier divergences that would occur if the air ionization from the transmission lines was far stronger than predicted, as well as signal strength fading effects that would be observable if the transmission lines were emitting interference in the L1 or L2 bands.

If air ionization effects were present, they would be observed as a change in the L1 minus L2 carrier phase observations as the ray path between the satellite and the user traversed the conductors of the transmission line, as well as the region between the conductors. If interference was emitted from the transmission lines, it would be observable as a decrease in the carrier-to-noise density ratio as the test vehicle approached the transmission lines, returning to normal as the vehicle passed to the other side of the transmission corridor. Since these effects would be most clearly discernable during a perpendicular test scenario, relevant results are presented in Figure 11.

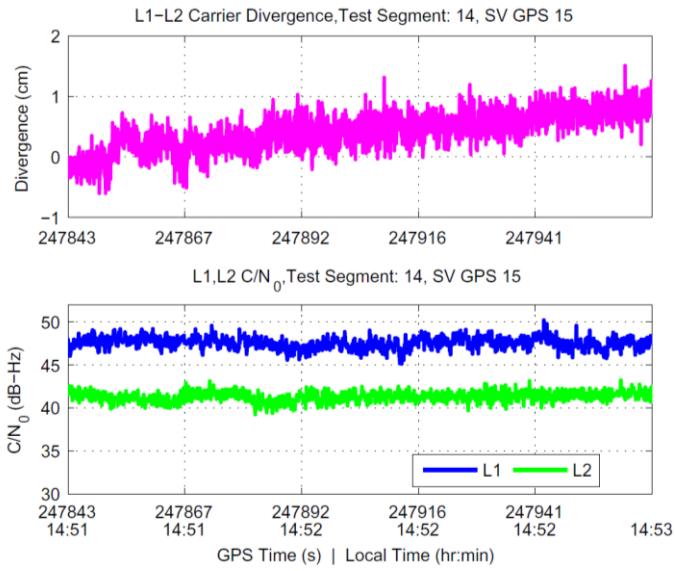

Figure 11 - L1–L2 carrier divergence and signal carrier strength of GPS PRN 15 during test segment 14. No anomalous behavior noted.

The signal characteristics presented indicate no abnormal features. No detectable RF interference is present in the GNSS navigation bands as evidenced by the nearly constant carrier signal strengths that show no noticeable reduction near the transmission lines. Additionally, the very slowly and smoothly varying carrier divergence measurement is indicative of normal background ionospheric effects, and shows no indication of a measurable effect due to air ionization adjacent to the transmission lines.

All perpendicular test trajectories produced similar null observations to those shown in Figure 11. Moving to the consideration of the carrier divergence and signal strength indicators produced during trajectories parallel to the transmission lines, deleterious effects were encountered. However, these are the result of mundane signal blockage or antenna gain pattern variations such as high vehicle dynamics requiring a 50% increase in GSNRx™ PLL bandwidth which causes a slight degradation of measurement quality. In addition, the deep fades typically associated with solid objects such as trees intersecting the ray path between a low elevation satellite and the user antenna are not due to interference from the transmission lines themselves.

Consistent changes in the carrier divergence of all satellites observed during parallel traversal tests are due to a phenomenon known as ‘carrier phase wind up’. Due to the circular polarization of GPS and GLONASS signals, rotation of the receiving antenna results in apparent carrier phase advance or retreat from the point of reception. In the case of the testing executed, the windup effect is due to one half of a left turn at the far point in each trajectory where the direction of the truck is reversed from north facing to south facing. This negative one half-cycle is equivalent to a phase observed range change of -9.75 cm of GPS L1 signal phase, and approximately -12.2 cm of GPS L2 phase. The theoretical L1-L2 difference as a result of the left turn would therefore be predicted as +2.45 cm of divergence, which appears to precisely match the observed change.

3.6 HSGPS Observations

The high sensitivity GPS receiver tested herein was not hindered and suffered no additional errors other than what would be expected in a single point GPS L1 only solution. Figure 12 shows the internal solution position accuracy and satellite geometry. In general, the single point navigation solution should be within a few metres and these results are no exception. Twelve satellites were tracked continuously and the HDOP was 0.8, which is extremely good for a GPS only receiver.

Shown explicitly in Figure 7, the receiver recorded similar power levels as that of the agricultural and survey grade receivers, as expected. Variations are expected based on the low noise amplifier and gain pattern of each antenna.

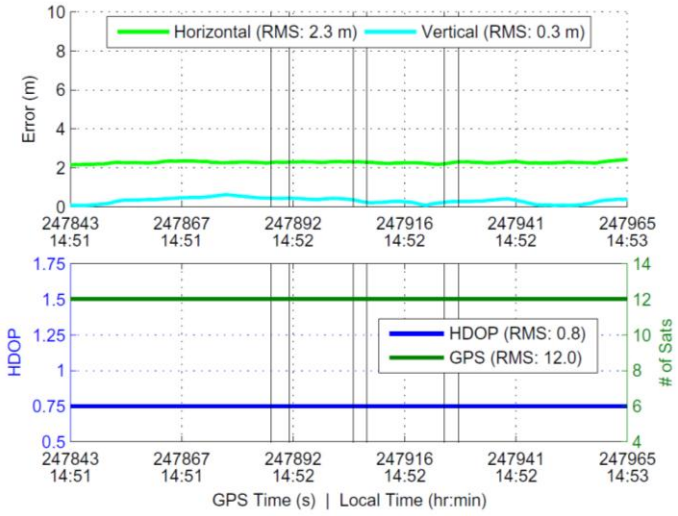

Figure 12 - Position error and satellite geometry (vertical lines represent time directly beneath transmission lines), receiver: u-blox Antaris 4, processed by: u-blox Internal Solution, data: L1 + HSGPS, test segment: 14.

4. Conclusions

GNSS data collected under two 500kV HVDC bipole lines were analyzed. Using two agricultural/survey grade GNSS receivers, a software based receiver and a high sensitivity GPS receiver, only non-impeding effects on the receivers or the L1 and L2 GNSS signals, in the form of cycle slips, were measured due to the transmission lines and their respective towers. Only a weak correlation between the location of the tower and the location of the cycle slips was observed. The cycle slips that did occur were so infrequent that the redundant measurements in the navigation solutions easily mitigated them. No transmission line effect on GNSS measurements was found to affect the quality of the navigation solutions. In addition, the test results showed normal operation of a commercially available survey grade RTK system and its radio link (450 MHz) for static and perpendicular test segments perpendicular to the transmission lines. Four different processing methods and software (GSNRx™, GrafNav, PLANSoft™, and the Trimble RTK solution) were able to provide consistent results (with the exception of the RTK solution which was not able to provide a real time fixed solution when the vehicle experienced high dynamics when driving off road). No adverse effects were measurable in the IF data as processed by GSNRx™. This paper analyzed the following metrics to form these conclusions:

1. Position Accuracy
2. HDOP
3. Number of Satellites
4. RMS of Code and Phase Residual errors
5. Location and Number of Cycle Slips
6. Carrier to Noise Density (and Average of all Satellites)
7. L1-L2 Carrier Divergence

References

Gelb, A., 1974. Applied Optimal Estimation. The Massachusetts Institute of Technology Press. Cambridge, Massachusetts.

IS-GPS-200E, 2010. Navstar GPS Space Segment/Navigation User Interface, Revision E., GPS Joint Program Office.

Juette, G.W., 1971. Evaluation of Television Interference from High-Voltage Transmission Lines. IEEE Summer Meeting and International Symposium on High Power Testing. Portland, OR, pp. 4.

Lundkvist, J., Gutman I. and Weimers, L. 2009. Feasibility study for converting 380 kV AC lines to hybrid AC / DC lines. EPRI's High-Voltage Direct Current & Flexible AC Transmission Systems Conference. Westminster, CO, pp. 11.

Morrison, A., 2010. High Latitude Ionospheric Scintillation: Detection and Isolation from Oscillator Phase Noise as Applied to GNSS, Ph.D. Thesis, Department of Geomatics Engineering, University of Calgary, Canada.

NovAtel Inc., 2010. NovAtel GPS 702 GG Antenna Data Sheet, pp. 2.

Pacific Gas and Electric, 2005. Pacific Gas and Electric Delta Distribution Planning Area capacity Increase Substation Project Proponent's Environmental Assessment: Section 16 Corona and induced current effects, No report number given, pp. 7.

Pawar, S.D., Murugavel, P., and Lal, D.M. 2009. Effect of relative humidity and sea level pressure on electrical conductivity of air over Indian Ocean. Journal of Geophysical Research, 114, D02205, pp. 8.

Petovello, M.G., O'Driscoll, C., Lachapelle, G., Borio, D. and Murtaza, H. 2009, Architecture and Benefits of an Advanced GNSS Software Receiver, Positioning, 1, 1, pp. 66-78.

Phaiboon, S., Vivek, V. and Somkuarnpanit, S. 2000. Analysis and Measurement of Radio-Frequency Interference Due to the Corona From 500kV Transmission Lines, TENCON 2000, Kuala Lumpur , Malaysia pp. 88-91.

Phillips, D., 2007. Corona Tutorial, Presented at IEEE Joint Technical Committee Meeting, San Diego CA, pp. 22.

Sadiku, M.N.O., 2001. Elements of Electromagnetics Third Edition. Oxford University Press, New York, NY.

Silva, J.M., 2002. Evaluation of the Potential for Power Line Noise to Degrade Real Time Differential GPS Messages Broadcast at 283.5-325 kHz, IEEE Transaction on Power Delivery, 17, 2, pp. 326-333.

Silva, J.M. and Olsen, R.G. 2002. Use of Global Positioning System, GPS, Receivers Under Power-Line Conductors, IEEE Transactions on Power Delivery, 17, 4, pp. 938-944.